THE JOURNAL OF PHYSICAL CHEMISTRY B

Article

pubs.acs.org/JPCB

Patterning Poly(dimethylsiloxane) Microspheres via Combination of Oxygen Plasma Exposure and Solvent Treatment

Qiaoyuan Li,[†] Xue Han,[†] Jing Hou,[†] Jian Yin, Shichun Jiang, and Conghua Lu*

School of Materials Science and Engineering, Tianjin University, Tianjin 300072, People's Republic of China

Supporting Information

ABSTRACT: Here a simple low-cost yet robust route has been developed to prepare poly(dimethylsiloxane) (PDMS) microspheres with various surface wrinkle patterns. First, the aqueous-phase-synthesized PDMS microspheres are exposed to oxygen plasma (OP), yielding the oxidized SiO_x layer and the corresponding stiff shell/compliant core system. The subsequent solvent swelling and solvent evaporation induce the spontaneous formation of a series of curvature and overstress-sensitive spherical wrinkles such as dimples, short rodlike depressions, and herringbone and labyrinth patterns. The effects of the experimental parameters, including the radius and Young's modulus of the microspheres, the OP exposure duration, and the nature of the solvents, on these tunable spherical wrinkles have been systematically studied. The experimental results reveal that a power-law dependence of the wrinkling wavelength on the microsphere radius exists. Furthermore, the induced wrinkling patterns are inherently characteristic of a memory effect and good reversibility. Meanwhile, the corresponding phase diagram of the wrinkle morphologies on the spherical surfaces vs the normalized radius of curvature and the excess swelling degree has been demonstrated. It is envisioned that the introduced strategy in principle could be applied to other curved surfaces for expeditious generation of well-defined wrinkle morphologies, which not only enables the fabrication of solids with multifunctional surface properties, but also provides important implications for the morphogenesis in soft materials and tissues.

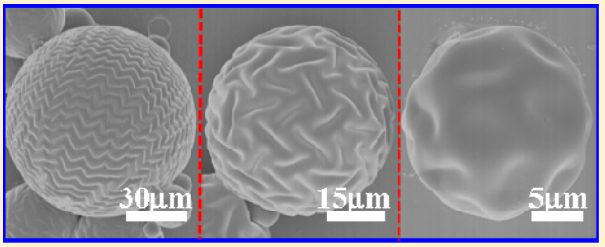

INTRODUCTION

Spontaneous formation of surface wrinkling patterns has attracted increasing attention because of their potential applications ranging from microlens arrays[1,2] to thin film property metrology,[3,4] stretchable electronics,[5,6] and nonlithographic microstructured templates.[7,8] It is well accepted that surface wrinkling frequently happens on a bilayer system with a thin stiff film attached to a relatively thick compliant substrate, when the bilayer is subjected to in-plane compression. The sinusoidal undulations would appear in the film surface once the induced compressive stress σ exceeds the critical wrinkling stress σ_c.[9] Here σ mainly originates from the bilayer strain mismatch during the in-plane compression and is usually achieved by thermal expansion, mechanical stretching, and solvent swelling. On the basis of the principle of minimizing the system potential energy, the characteristic critical wrinkling wavelength λ and critical wrinkling stress σ_c are determined by $\lambda = 2\pi h(\bar{E}_f/3\bar{E}_s)^{1/3}$ and $\sigma_c = (\bar{E}_f/4)(3\bar{E}_s/\bar{E}_f)^{2/3}$, respectively.[9,10] Here h is the film thickness, $\bar{E} = E/(1-\nu^2)$ is the plane-strain modulus, E is Young's modulus, and ν is Poisson's ratio. The subscripts f and s represent the film and substrate, respectively.

Since the pioneering work of Bowden et al.,[10] considerable efforts have been made to manipulate the wrinkled morphologies in planar film/substrate systems. A high degree of regularity and controllability of surface wrinkling patterns have been pursued in the past two decades. Given the stress-relief mechanism, the elaborate creation of a local stress/strain field is a familiar strategy to tune the wrinkling patterns, which could always be implemented by a prepatterned substrate[11,12] or film.[5,13,14] In addition, alternative innovative methods have also been employed, such as external mold confinement,[15] direct writing of a laser,[16] or a focused ion beam,[17,18] allowing the controlled fabrication of surface wrinkles more flexibly.

In fact, many natural and industrial surface wrinkling phenomena often happen on nonplanar substrates, for instance, the aging of human skin, some dehydrated fruits and vegetables.[9,19] Owing to geometric constraints, surface wrinkling behaviors on curved surfaces can be quite different from those on planar ones.[19−31] Among them, a spherical surface as a typical curved surface has been used to study nonplanar wrinkling both theoretically and experimentally.[20,23,24,26−31] Theoretical predictions such as the finite element method or the volumetric growth theory of finite deformation explicitly reveal that the selected wrinkling patterns are sensitive to the normalized substrate radius of curvature R/h_R and the overstress σ^R/σ_c^R. For example, triangular dentlike, ordered dimples or buckyball-like wrinkling patterns preferentially appear on the spherical surfaces in the case of a smaller R/h_R, a bigger Ω, or a smaller σ^R/σ_c^R (or $\bar{g}$), whereas typical labyrinth morphologies are mainly self-

Received: July 25, 2015
Revised: September 8, 2015
Published: October 4, 2015

DOI: 10.1021/acs.jpcb.5b07208
J. Phys. Chem. B 2015, 119, 13450−13461

assembled in the case of a larger R/h_R, a smaller Ω, or a larger σ^R/σ_c^R (or $\bar{g}$).[20,23,31] Here σ^R and σ_c^R denote the applied stress and the critical wrinkling stress on a spherical core/shell system with shell thickness h_R and substrate radius R, respectively. $\bar{g}$ is the growth/shrinking factor.[23] Ω is the introduced dimensionless curvature parameter,[26] which is defined as[32]

$$\Omega = 2\sqrt{(1-\nu_f^2)}\,(h_R/R)\left(\frac{\bar{E}_f}{3\bar{E}_s}\right)^{2/3} \quad (1)$$

Then σ_c^R can be determined by[32]

$$\frac{\sigma_c^R}{\sigma_c} \approx 1 + \Omega^2 \quad (2)$$

According to eqs 1 and 2, it is seen that σ_c^R is intimately dependent on R/h_R and $\bar{E}_f/\bar{E}_s$.

This curvature and overstress-sensitive surface wrinkling behavior has been verified in a series of experimental systems.[20,23,24,26−30] Cao et al.[20] prepared Ag core/SiO_2 shell spherical microstructures via thermal coevaporation of precursor powers at high temperature. Upon cooling, triangular dentlike patterns prevailed on the small particles, while labyrinthlike patterns took over on the larger particles. Li et al.[23] observed that fresh green peas, which are considered as a spherical seed covered by a harder shell, initially shrunk isotropically, followed by evolution into buckyball-like wrinkling patterns and finally a labyrinth-like wrinkle morphology during drying. Trindade et al.[24] synthesized polyurethane/polybutadiene (PU/PBDO) composite spheres, which were subjected to UV irradiation, solvent swelling, and drying. Thus, labyrinthine wrinkling patterns and even hierarchical micro/nanostructures[33] were readily triggered on these elastomeric composite spheres, forming Janus particles with asymmetric morphologies. Jeong et al.[27] utilized spherical wrinkling as a probe for characterization of the mechanical properties of a gold nanoparticle monolayer, which self-assembled at the oil/water interface and was cross-linked by linkers using specific host−guest chemistry. After solidification of the inner oil phase via polymerization, volume shrinkage induced the spontaneous formation of spherical wrinkles. Additionally, Terwagne et al.[28] combined rapid prototyping with coating and casting to fabricate silicone-based polymer core/shell spherical specimens, and the interior of the core contained a cavity that was connected to a pneumatic system. Upon depressurization, homogeneous compression excited an undulatory wrinkled morphology on the shell. Recently, Bae et al.[30] incubated UV-polymerized microparticles into the solution for a silica-coating reaction, forming a core/shell structure. The mismatched strain induced by subsequent drying of these particles resulted in the labyrinth wrinkle patterns, which were called artificial microfingerprints and were applicable to anticounterfeiting strategies.

Despite successful creation of surface wrinkles on spherical surfaces by the above-mentioned technical routes, some intrinsic limitations have been identified in these methods. For example, the Ag core/SiO_2 shell spherical system required a high temperature,[20] and spherical wrinkling was triggered only on hemispherical surfaces in the PU/PBDO Janus spheres.[24,33] The formation of nanoparticle monolayer films needed an elaborate design of interactions between the nanoparticles and linkers based on the host−guest chemistry.[27] As for the silicone-based polymer core/shell system, it relied on an extra polystyrene hemispherical mold and a laser-cut and 3D-printed scaffold, and the wrinkling wavelength had no dependence on the substrate radius due to the large radius of curvature on the millimeter scale.[28] Other attempts have been established, including suspension polymerization,[34] multistep seeded swelling polymerization,[35] and interfacial instabilities of emulsion droplets,[36] to generate polymer microparticles with wrinkled surfaces. Nevertheless, these methods could not be directly transferred to nonspherical substrates.

Throughout the development of surface wrinkling on planar surfaces, poly(dimethylsiloxane) (PDMS) as a soft compliant substrate has been paid close attention due to its fine flexibility, transparency, and nontoxicity.[9] However, PDMS as a curved substrate to investigate nonplanar wrinkling behaviors has rarely been reported. Thereinto, Breid et al.[26] explored surface wrinkling in the supported spherical caps of PDMS accompanied by ultraviolet/ozone (UVO) treatment and solvent vapor swelling, and the wrinkling patterns on the PDMS spherical caps easily disappeared upon solvent evaporation. Recently, our group[29] systematically investigated spherical wrinkling on the basis of surface chemical oxidation of aqueous-phase-synthesized PDMS microspheres in a mixed $H_2SO_4/HNO_3/H_2O$ solution. Despite the high controllability of spherical wrinkling in the PDMS microsphere system, a strongly corrosive acid mixture was utilized, and the correlation of the wrinkling wavelength with the shell thickness has not been obtained yet. Therefore, systematic investigation on the correlation of nonplanar wrinkling behaviors with the mechanical parameters of the film/substrate bilayer and the film thickness is still lacking. Furthermore, it remains a challenge to develop a simple low-cost yet robust approach for surface wrinkling on curved substrates from a scientific and technical point of view.

In this paper, we report surface wrinkling behaviors on PDMS microspheres with typically nonplanar surfaces via the combination of oxygen plasma (OP) exposure and solvent swelling. OP treatment of PDMS microspheres creates a thin stiff oxidized SiO_x shell,[13,14,37−40] forming the required modulus mismatch of surface wrinkling. Subsequent solvent swelling/evaporation induces a series of curvature and overstress-sensitive wrinkle morphologies, including ordered dimples, short rodlike depressions, and labyrinth and herringbone wrinkled patterns. Note that few reports have predicted and demonstrated herringbone wrinkles on curved surfaces theoretically and experimentally.[26] Additionally, as a commonplace surface modification approach for the PDMS substrate, OP exposure has been widely employed in the investigation of PDMS-based planar wrinkling.[13,14,37−40] However, to the best of our knowledge, no study takes advantage of OP exposure for spherical wrinkling. The influences of the experimental parameters, including the radius and Young's modulus of PDMS microspheres, the OP exposure duration, and the solvent nature, on the spherical wrinkling behaviors have been systematically studied. Compared with the previous techniques,[20,23,24,26−30,33] the present method is inherently simple, safe, rapid, and cost-effective. Here we have captured the quantitative correlation of the wrinkling wavelength with the SiO_x shell thickness. It is strongly believed that surface wrinkling behaviors on nonplanar substrates will not only benefit important implications for the morphogenesis in soft materials and tissues,[19,25] but also open a new avenue for the fabrication of intriguing patterns on curved surfaces and further microcomponents with augmented functionalities, which are inaccessible for other patterning techniques.

DOI: 10.1021/acs.jpcb.5b07208
J. Phys. Chem. B 2015, 119, 13450−13461

EXPERIMENTAL SECTION

Materials. The base/curing agent (Sylgard 184) PDMS was purchased from Dow Corning Corp. Poly(vinyl alcohol) (PVA; M_w = 20000−30000, 88+% hydrolyzed) was purchased from J&K Scientific Ltd. Methyl methacrylate (MMA), cyclohexane, toluene, acetone, and ethanol were purchased from Jieerzheng Chemical Industry Trade Corp., Ltd. (Tianjin, China).

Synthesis of PDMS Microspheres. Synthesis of PDMS$_{(n:1)}$ microspheres with a designed weight ratio (n:1) of base to curing agent was carried out in an aqueous solution according to our previous paper.[29] Roughly, the mixed base/curing agent at an n:1 ratio (e.g., n:1 = 10:1, 15:1, 20:1, 30:1, and 40:1) was stirred thoroughly, followed by degassing for 30 min. Then 0.6 g of the above base/curing agent mixture and 30 mL of 15 wt % PVA aqueous solution were added to a Teflon reaction kettle in sequence. The formed emulsion droplet was stirred vigorously at room temperature for 12 h and then at 80 °C for another 12 h to complete the curing reaction. The as-synthesized PDMS microspheres were centrifuged at 3000 rpm and washed with distilled water several times.

Surface Wrinkling on PDMS$_{(n:1)}$ Microspheres via Combination of Oxygen Plasma Exposure and Solvent Swelling. The as-washed PDMS$_{(n:1)}$ microspheres were deposited on a clean glass slide first. Then the microspheres were exposed to OP (Harrick PDC 32G) at a pressure of 0.2 mbar with a medium rf power (10.5 W) for a certain duration, t_{OP}. After OP treatment, the microsphere-coated glass slide was carefully immersed into an organic solvent for a certain duration, followed by drying in the ambient atmosphere.

Characterization. The as-prepared PDMS microspheres before and after the combined OP/solvent treatment were characterized by field-emission scanning electron microscopy (SEM) (Hitachi S4800). Before SEM characterization, a Pt film was sputtered with an E-1045 ion sputter (Hitachi) at a pressure of 7 Pa and a current of 15 mA. The in situ optical observation of morphological evolution of the PDMS microspheres during solvent processing was performed on an inverted Observer A1 microscope (Zeiss, Germany) equipped with a charge-coupled device camera. The stress−strain curves of the PDMS planar films with different n:1 ratios before and after solvent extraction were measured on a Linkam TST-350 tensile stress tester (Linkam Scientific Instruments, Ltd., United Kingdom).

RESULTS AND DISCUSSION

Figure 1 illustrates the schematic procedure to trigger the curvature and overstress-sensitive surface wrinkling on PDMS microspheres. Typically, the as-synthesized PDMS$_{(n:1)}$ microspheres from different weight ratios (n:1) of base to curing agent were first predeposited on a clean glass slide and then subjected to OP exposure for a certain duration, t_{OP} (Figure 1, step I). Subsequently, the glass slide with OP-treated PDMS$_{(n:1)}$ microspheres was carefully immersed into an appropriate organic solvent (Figure 1, step II), followed by air drying at room temperature (Figure 1, step III).

As for the PDMS$_{(n:1)}$ microspheres, they were synthesized in an aqueous solution according to our previous paper.[29] The SEM image indicates that these water-washed PDMS$_{(30:1)}$ microparticles obviously possess spherical morphologies with smooth surfaces (Figure 2a). Meanwhile, the radius distribution for the PDMS$_{(30:1)}$ microspheres is relatively dispersive, compared to that of microfluidic-synthesized PDMS microbeads.[41] However, this polydispersity in the PDMS microsphere radii benefits our one-pot investigation of the influence of substrate curvature on surface wrinkling behaviors from another perspective. In other words, the aqueous-phase synthesis method of PDMS microspheres not only is simple and accessible to a general laboratory, but also provides satisfactory spherical substrates to uncover the correlation of substrate curvature with surface wrinkling morphologies and their feature characteristics. Similarly, PDMS$_{(n:1)}$ microspheres with other n:1 ratios (e.g., n:1 = 10:1, 15:1, 20:1, and 40:1) have also been successfully prepared (Figure S1). As displayed in Figure S1, smooth isolated PDMS microspheres could be obtained when n:1 ranges from 10:1 to 20:1, whereas with a further increase of n:1 to 40:1, microsphere aggregations become apparent and the adhesion of intermicrospheres leads to severe deformation owing to a low cross-linking density from a high weight ratio of base to curing agent. At this point, it could be envisioned that PDMS$_{(30:1)}$ microspheres retain their intrinsic smooth morphologies and offer enough flexibility as soft substrates applicable to the subsequent core/shell spherical wrinkling.

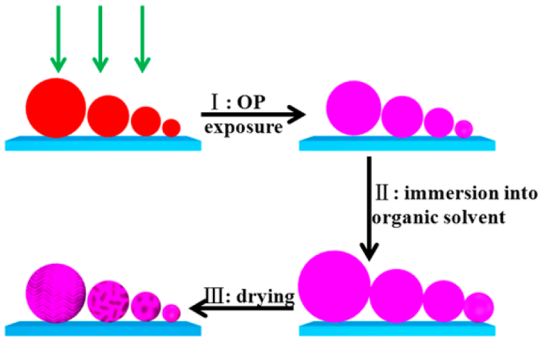

Figure 1. Schematic illustration of the experimental procedure for surface wrinkling on PDMS microspheres, i.e., OP exposure of PDMS microspheres that are predeposited on a glass slide (I), followed by immersion into an appropriate organic solvent (II) and subsequent drying in the atmosphere (III).

It is well accepted that OP treatment is a commonplace surface modification approach for the PDMS substrate, which has been widely employed in the investigation of the planar film/substrate wrinkling.[13,14,37−40] In the current case, the exposure of PDMS microspheres to OP results in the conversion of the microsphere surface into a thin stiff oxidized silica-like (SiO_x) layer,[13,14,37−40] creating the modulus contrast between the shell and the core required for the spherical wrinkling. Figure 2b shows that the OP-exposed PDMS$_{(30:1)}$ microspheres with the shell/core structures still keep the smooth surface, similar to the original as-synthesized microspheres (Figure 2a).

When the OP-exposed PDMS$_{(30:1)}$ microspheres were immersed into the solvent MMA and then dried in the air, the initial smooth surface became rough, just as shown in Figure 2c−f. The SEM images clearly demonstrate that surface microtextures with typical wrinkle morphologies have been induced spontaneously on the shell/core microspheres (Figure 2c−f). Furthermore, the wrinkled patterns on the spherical surfaces are strongly dependent on the microsphere radius R. For example, when R increases from ∼9.75 to 56.07 μm, the corresponding wrinkles change from dimples (or buckyball-like) (Figure 2f) to short rodlike depressions (Figure 2e) and finally evolve into herringbone patterns (red dotted circle in Figure 2c). Here the observed short rodlike depressions could

DOI: 10.1021/acs.jpcb.5b07208
J. Phys. Chem. B 2015, 119, 13450−13461

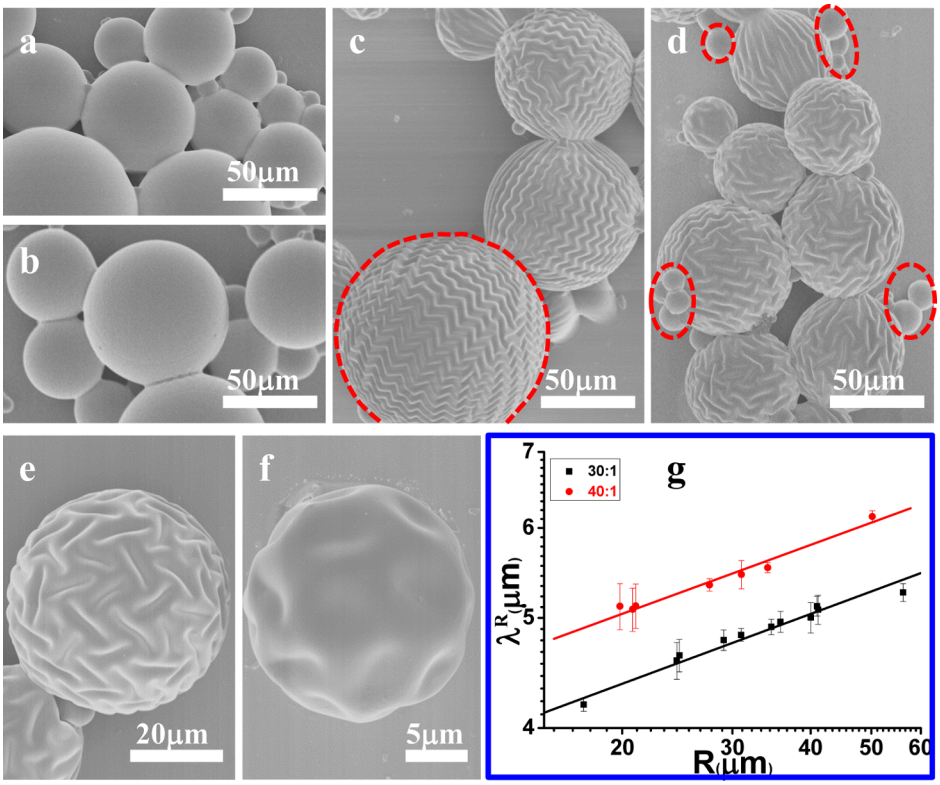

Figure 2. SEM images of $PDMS_{(30:1)}$ microspheres before OP exposure (a) and after OP exposure for t_{OP} = 10 min (b) followed by MMA swelling (c–f). Zoomed $PDMS_{(30:1)}$ microspheres with radius $R \approx$ (e) 24.41 μm and (f) 9.75 μm. Frame g shows the λ^R–R relationship for $PDMS_{(30:1)}$ and $PDMS_{(40:1)}$ microspheres.

be considered as the further coalescence of the dimples and could narrow into troughs.[23] As for the herringbone wrinkle patterns, they are rarely predicted or achieved on spherical substrates both theoretically and experimentally, in spite of the energetically preferential appearance of herringbone patterns on planar film/substrate systems in the case of the equi-biaxial stress state.[32] Under the same conditions, no surface wrinkling is triggered on a small-radius $PDMS_{(30:1)}$ microsphere (red dotted circles in Figure 2d), owing to the great increase in the critical wrinkling stress σ_c^R for a small radius R or a large curvature parameter Ω according to eqs 1 and 2.[26,32] Figure 2g shows the relation of the wrinkling wavelength λ^R to the microsphere radius R. Here λ^R is extracted from the recorded SEM images. It is found that, in the double logarithmic coordinate system, λ^R and R exhibit a power-law relation (Figure 2g).

In the above procedure, a SiO_x shell/PDMS core spherical system is generated after OP exposure of the PDMS microspheres. To clarify the mechanism of spherical wrinkling here, we performed an in situ optical observation of these OP-exposed PDMS microspheres, recording the morphological evolution of the PDMS microspheres from dropping of a droplet of MMA (~5 μL) to subsequent MMA volatilization on the microsphere surface (Figure S2 and Movie S1). After a droplet of MMA is dropped, the OP-exposed PDMS microsphere is swollen immediately, and the microsphere surfaces in the swelling state remain smooth, indicative of the absence of the surface wrinkling in this step. Meanwhile, Movie S1 shows that the swelling step of the microsphere lasts less than 2 min. We believe that the short swelling time coupled with the small droplet of MMA results in few uncured molecules extracted from the PDMS core by the swelling solvent MMA. Here r_D is introduced to estimate the rate of the diameter change with $r_D = (D - D_0)/D_0 \times 100$, where D_0 and D are the microsphere diameters before and after the MMA swelling, respectively. Under the specified conditions, D also represents the diameter after the solvent evaporation. Thus, the positive/negative r_D stands for the increase/decrease in the microsphere diameter and the corresponding volume swelling/shrinking, respectively. Figure 3a further shows that the PDMS microsphere diameters are almost constant after drying in the case of dropping MMA, again confirming that few uncured molecules have been extracted from the PDMS cores in the swelling step. However, the wrinkles indeed emerge on the microsphere surface and are stable in long-term storage. This strongly illustrates that the extraction of uncured molecules and the resulting volume decrease in the PDMS core are not the key steps in the fabrication of wrinkled PDMS microspheres. Considering the whole process, it is expected that what plays a dominant role in the surface wrinkling is the swelling degree of the PDMS microspheres. Namely, owing to the swelling coefficient of the PDMS core in MMA being higher than that of the SiO_x shell, the final air-drying step leads to a buildup of internal stress, which is an equi-biaxially compressive hoop stress σ^R for the SiO_x outer shell. Once σ^R is higher than the critical spherical wrinkling stress σ_c^R, surface wrinkling with well-ordered periodical wrinkles happens on spherical surfaces (Figure 2, Figure S2, and Movie S1). The resulting characteristic wrinkling wavelength is determined by the competition between the bending stiffness of the thin shell (which penalizes short wavelengths) and the bulk elastic energy of core deformation (which penalizes long wavelengths). Thus, solvent swelling of a soft substrate constrained by a stiff thin surface

DOI: 10.1021/acs.jpcb.5b07208
J. Phys. Chem. B 2015, 119, 13450–13461

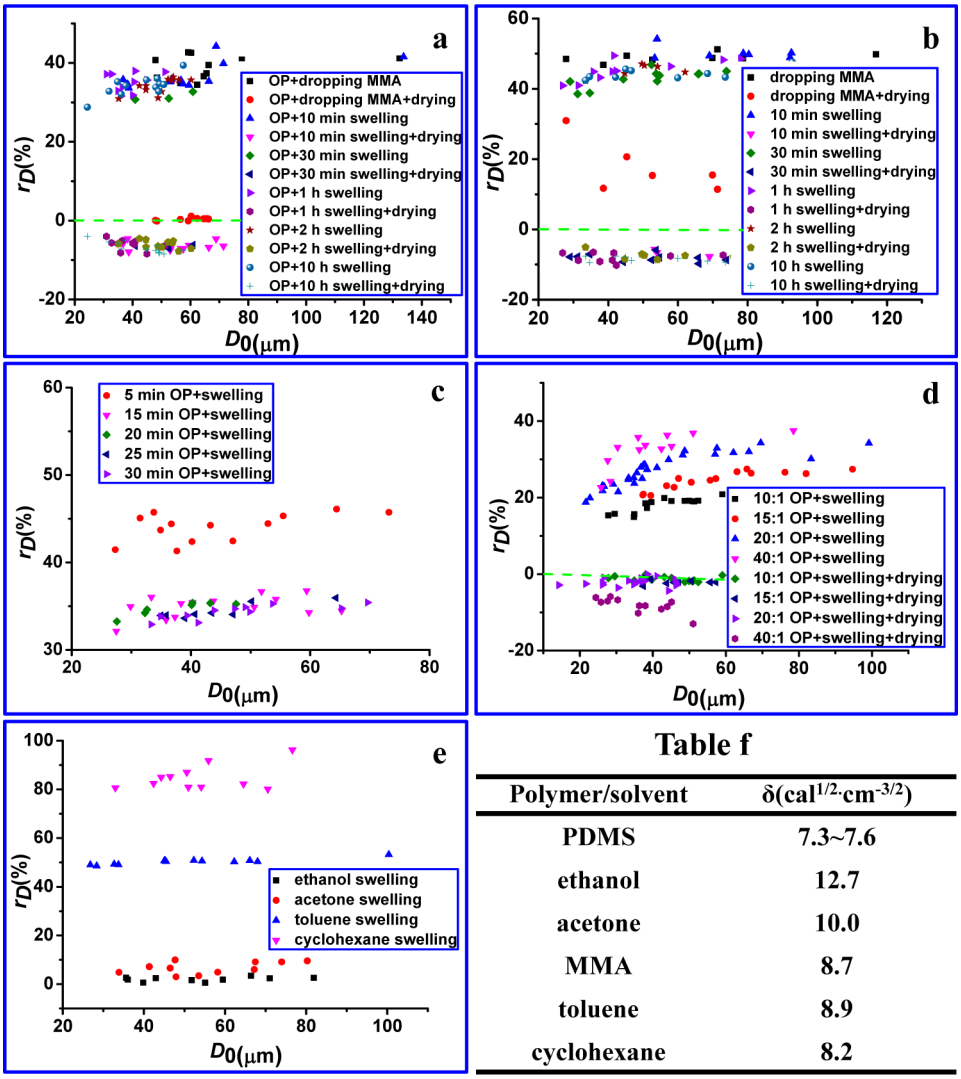

Table f

Polymer/solvent	δ(cal$^{1/2}$·cm$^{-3/2}$)
PDMS	7.3~7.6
ethanol	12.7
acetone	10.0
MMA	8.7
toluene	8.9
cyclohexane	8.2

Figure 3. (a–e) Rate of the diameter change (r_D) of PDMS$_{(n:1)}$ microspheres during solvent swelling and air drying as a function of the microsphere diameter D_0. (a) OP-exposed PDMS$_{(30:1)}$ microspheres with t_{OP} = 10 min followed by dropping of MMA or MMA swelling in the beaker for different applied durations. (b) Original PDMS$_{(30:1)}$ microspheres after dropping of MMA or MMA swelling in the beaker for different applied durations. (c) OP-exposed PDMS$_{(30:1)}$ microspheres for different t_{OP} values after MMA swelling. (d) OP-exposed PDMS$_{(n:1)}$ microspheres for t_{OP} = 10 min after MMA swelling. (e) OP-exposed PDMS$_{(30:1)}$ microspheres for t_{OP} = 10 min after swelling with different organic solvents. Table f lists the solubility parameter (δ) of the involved organic solvents and PDMS.

layer is convenient and robust for nonplanar geometries to give rise to wrinkle morphologies.

This is easily reminiscent of the work of Trindade et al.,[24] in which PU/PBDO composite spheres were subjected to UV irradiation to form a thin stiff surface layer, followed by toluene swelling and subsequent drying. Finally, labyrinthine wrinkles are induced on the UV-exposed zones of the composite spheres. It is demonstrated that surface wrinkling on these composite spheres is mainly attributed to the swelling of toluene into these spheres, especially emphasizing in the Experimental Section that "a Soxhlet apparatus was used to extract the spheres in toluene for 36 h at 60 °C" before UV irradiation. We believe that they employ this process to extract uncured molecules in advance. Therefore, in their experimental system, the swelling degree of the composite spheres is the main source of the required compressive stress, which can also be inferred from their established analytical mode. It can be seen that our current system has a lot in common with theirs, and it is reasonable to expect that the swelling degree of PDMS microspheres, rather than the extraction of uncured molecules from PDMS cores, plays a decisive role in the surface wrinkling.

Additionally, we also examine the diameter variation of the OP-exposed PDMS microspheres with the immersion time in the swelling agent MMA (Figure 3a). We find that the r_D of these microspheres decreases by ~10% no matter what the immersion time is, which is obviously attributed to the extraction of uncured molecules from the PDMS cores. More specifically, if the method of dropping solvents to induce spherical wrinkling is employed, the swelling degree of the PDMS microspheres is responsible for the compressive stress due to little extraction of uncured molecules from the PDMS core; if PDMS microspheres are immersed in MMA, the compressive stress results from two things: one is the swelling degree of the PDMS microspheres, and the other is volume shrinkage from extraction of uncured molecules. Despite this, the swelling degree of the PDMS microspheres is still the key step in the fabrication of wrinkled PDMS microspheres and determines the magnitude of compressive stress and the final

DOI: 10.1021/acs.jpcb.5b07208
J. Phys. Chem. B 2015, 119, 13450–13461

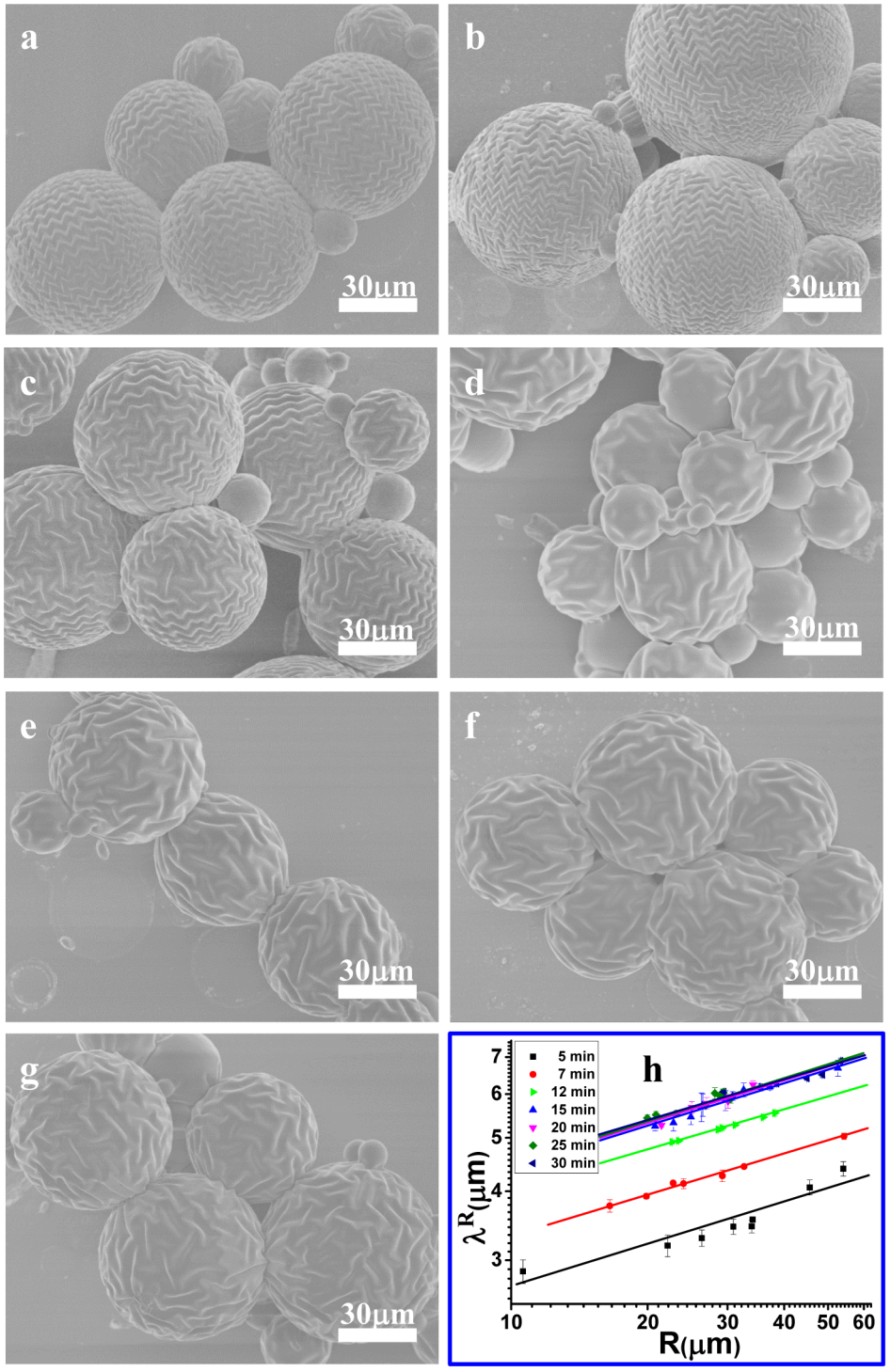

Figure 4. SEM images of MMA-treated $PDMS_{(30:1)}$ microspheres with different t_{OP} values: (a) 5 min, (b) 7 min, (c) 12 min, (d) 15 min, (e) 20 min, (f) 25 min, and (g) 30 min. Frame h shows the λ^R–R relationship for $PDMS_{(30:1)}$ microspheres from different t_{OP} values.

wrinkle patterns. Moreover, the r_D of the PDMS microspheres without OP exposure in the swelling state (~40–50%) is slightly larger than that of the corresponding OP-exposed PDMS microspheres (~30–40%) due to the absence of constraint from the SiO_x outer shell (Figure 3a,b). Similar to that of the OP-exposed PDMS microspheres, the r_D of PDMS microspheres without OP exposure after drying also decreases by ~10% regardless of the immersion time (Figure 3b). This illustrates that the uncured molecules are easily extracted from the PDMS microspheres and further reach an equilibrium state in the organic solvent. It is noteworthy that if the method of dropping solvents is employed, the r_D of the PDMS microspheres increases after drying and is even up to ~30% sometimes, which originates from the collapse of the PDMS microspheres due to the leakage of uncured molecules inside the PDMS microspheres. However, this is not observed in the case of OP-exposed PDMS microspheres, which demonstrates that the formed SiO_x shell can resist the leakage of uncured molecules from the PDMS cores to some extent and retains the complete spherical geometry.

DOI: 10.1021/acs.jpcb.5b07208
J. Phys. Chem. B 2015, 119, 13450–13461

After the OP exposure for the same duration (e.g., t_{OP} = 10 min), the shell thickness h_R of the induced SiO_x layer can be assumed to be equal for different radii of $PDMS_{(30:1)}$ microspheres. Thus, in Figure 2c–f, the dimple patterns prevail on the OP-exposed $PDMS_{(30:1)}$ microspheres with a smaller R/h_R or a larger Ω, whereas ridge-based wrinkle patterns such as herringbone patterns take over in the case of a larger R/h_R or a smaller Ω. These substrate curvature-sensitive wrinkle morphologies are consistent with the previously reported experimental and theoretical results.[20,23,26,29,31] Note that the herringbone patterns are induced on the microspheres with a larger R/h_R (circled in Figure 2c), which is rarely seen in the spherical wrinkling. Simultaneously, the underlying power-law behavior between λ^R and R is as well in good agreement with the previous results.[20,21,24,29] For instance, on the basis of the numerical simulation result of Yin et al.,[21] the critical wrinkling wavelength λ^R in a cylindrical substrate is determined by

$$\lambda^R = 2\pi h_R \left(\frac{R}{h_R}\right)^{1/4} \left(\frac{\bar{E}_f}{12\bar{E}_s}\right)^{1/4} \tag{3}$$

This can be further reduced to

$$\lg \lambda^R = \frac{1}{4} \lg R + C_1 \tag{4}$$

With respect to the result of Cao et al.,[20] the power-law relationship between λ^R and R for the (SiO_2) shell/(Ag) core microspheres is established by $\lambda^R/R = a(R/h_R)^b$ with constants a = 3.0 and b = −0.8, respectively. Therefore, we can acquire

$$\lg \lambda^R = \frac{1}{5} \lg R + C_2 \tag{5}$$

The experimental result of Trindade et al.[24] on the hemispherical surface wrinkling of a PU/PBDO composite microsphere gives

$$\lg \lambda^R = 0.18 \lg R + C_3 \tag{6}$$

In our recent paper on PDMS microspheres with spherical wrinkles initiated by surface chemical oxidization in a strong acid mixture,[29] the obtained λ^R and R approximately satisfy

$$\lg \lambda^R = 0.3 \lg R + C_4 \tag{7}$$

Among eqs 4–7, C_i (i = 1, 2, 3, 4) is a function of the shell thickness h_R and the modulus mismatch between the shell and the core, $\bar{E}_f/\bar{E}_s$. In the current case (i.e., h_R and $\bar{E}_f/\bar{E}_s$ remain constant from the same exposure duration t_{OP}), the relation between λ^R and R is well fitted as

$$\lg \lambda^R = 0.2 \lg R + 0.38 \tag{8}$$

It can be seen that the slope in eq 8 is apparently comparable to those shown in eqs 4–7. The slight differences among the slope values in eqs 4–8 can be ascribed to different surface wrinkling systems and the corresponding experimental conditions. Additionally, besides the experimental spherical system and the theoretical cylindrical system, a partial deviation of the slope from the theoretical prediction is presumably due to the fact that the OP exposure introduces a gradient SiO_x layer rather than a homogeneous layer with a constant elastic property,[13,14,37–40] as is frequently involved in the theoretical models. Certainly, on the basis of eqs 3 and 8, we can calculate the effective thickness h_R of the SiO_x layer formed on OP-exposed $PDMS_{(30:1)}$ microspheres with different R values for t_{OP} = 10 min. For example, when R is 56.21 and 17.35 μm, the corresponding h_R is estimated to be ∼12.62 and ∼ 12.75 nm, respectively. These results imply that the oxidized layer thickness induced by OP exposure is basically independent of the microsphere size. Here E_f = 40 GPa, ν_f = 0.33, E_s = 0.12 MPa, and ν_s = 0.5. Additionally, these estimated h_R values are the acceptable ones according to the previous literature.[37]

According to eqs 1–3, it is known that the shell thickness h_R has an important effect on the curvature R/h_R (or Ω), the critical wrinkling stress σ_c^R, the overstress σ^R/σ_c^R, and the resulting wrinkle morphologies and λ^R. This curvature and overstress-dependent spherical wrinkling behavior is evidently different from that in the planar case. Here, considering the thickness of the OP-exposure-induced SiO_x layer proportional to t_{OP}, we systematically investigate the influence of t_{OP}. The results shown in Figure 4 demonstrate that the surface wrinkling feature from other t_{OP} values (i.e., t_{OP} = 5, 7, 12, 15, 20, 25, and 30 min) is analogous to that from t_{OP} = 10 min (Figure 2c–f). Just as expected from eqs 1–3, it is difficult to trigger surface wrinkling on a relatively small $PDMS_{(30:1)}$ microsphere with a thicker shell (i.e., a larger t_{OP}) because of the increase of the critical wrinkling stress σ_c^R with the shell thickness h_R.[26,32] As for the approximately same radii of $PDMS_{(30:1)}$ microspheres, the bridged dimples and short rodlike depressions dominate on the microspheres from a larger t_{OP}. This could also stem from the increase of σ_c^R and the simultaneous decrease of σ^R with a thicker shell and the final decrease of the overstress σ^R/σ_c^R.[20,23,31]

Meanwhile, the diameter change of the $PDMS_{(30:1)}$ microspheres with t_{OP} in the swelling state is shown in Figure 3a,c. It can be seen that the thicker the SiO_x layer (i.e., t_{OP} is bigger), the more severe the constrained swelling becomes. Basically, the larger the swelling extent of the OP-treated PDMS microspheres, the larger the induced compressive stress in the shell/core spherical system correspondingly. Thus, it can be concluded that the compressive stress σ^R induced on the $PDMS_{(30:1)}$ core/shell microspheres increasingly decreases with t_{OP}, especially in the range of 5–15 min. The decrease of σ^R combined with the increase of σ_c^R with t_{OP} leads to the final decrease of the overstress σ^R/σ_c^R and eventually directs the emergence of bridged dimples and short rodlike depressions readily on the microspheres from a larger t_{OP}.

Figure 4h plots the dependence of the λ^R–R relation on the t_{OP}. Similar to the results for t_{OP} = 10 min given in Figure 2g, the power-law behavior between λ^R and R still exists for all other t_{OP} values. As mentioned above, h_R, which is implicitly involved in the constant C_i (i = 1, 2, 3, 4) of eqs 4–7, has nothing to do with the slope value. Namely, in the double logarithmic coordinate system, the λ^R–R plots from different t_{OP} values should be parallel to each other, as evidenced for t_{OP} = 5, 7, 10, 12, and 15 min in Figures 2g and 4h. Meanwhile, λ^R increases with t_{OP} when t_{OP} varies from 5 to 15 min. Nevertheless, further increasing t_{OP} (e.g., t_{OP} = 20, 25, and 30 min) has no obvious influence on λ^R, suggesting that a saturated thickness of the oxidized SiO_x layer arrives after t_{OP} > 15 min. The occurrence of the saturated thickness is attributed to a limited OP diffusion depth and the resistance of the as-formed SiO_x layer against the further OP diffusion.[13,14,37–40] In addition, the lg λ^R–lg R relation from different t_{OP} values is also plotted with the modified data in the linear coordinate system (Figure S3b). We also plot the relationship of λ^R versus t_{OP} from the same radius R (∼30 μm) (Figure S3a). It is seen that λ^R increases linearly with t_{OP} when 5 min ≤ t_{OP} ≤ 15 min in the

DOI: 10.1021/acs.jpcb.5b07208
J. Phys. Chem. B 2015, 119, 13450–13461

double logarithmic coordinate system and subsequently remains constant. This implies that the SiO_x layer thickness h_R likewise presents linear growth with t_{OP} when 5 min $\leq t_{OP} \leq$ 15 min and subsequently reaches a saturated value, while the modulus of the oxidized SiO_x layer changes little during the investigated t_{OP}. Our experimental results show good consistency with the literature reported previously,[11] in which the wavelength increases linearly with the oxidation time after the first 5 min. Recently, the reported frontal plasma conversion model[37] captured the logarithmic kinetics of film formation, which can be classified into three regimes, i.e., the induction regime, film formation regime, and film propagation regime. During the film formation regime, changes in the exposure duration will simultaneously affect the oxide thickness and modulus, resulting in a rapid increase of the wavelength. However, during the film propagation regime, changes in the exposure time primarily affect the film thickness, resulting in a subsequently slow increase of the wavelength. Thus, the film propagation regime could be roughly considered as slow linear growth of the thickness upon plasma exposure, basically similar to our experimental results in the range of 5−15 min. Meanwhile, this also confirms that here t_{OP} indeed primarily affects the film thickness and has little influence on the modulus of the SiO_x layer. Compared to the surface wrinkling on PDMS microspheres via wet surface chemical oxidation,[29] the characteristic wrinkle features could be accurately tuned by controlling t_{OP} and the corresponding h_R.

The influence of Young's modulus of $PDMS_{(n:1)}$ microspheres ($E_{PDMS(n:1)}$) on the wrinkling patterns is also investigated (Figure 5). In our experiment, $E_{PDMS(n:1)}$ can be well tailored by the cross-linking density of PDMS (i.e., the weight ratio n:1 of the base to curing agent). At the same time, $E_{PDMS(n:1)}$ can be roughly assumed equal to that of the corresponding planar film. On the basis of the measured stress−strain curves of solvent-extracted planar $PDMS_{(n:1)}$ films, $E_{PDMS(n:1)}$ of $PDMS_{(n:1)}$ microspheres is estimated to be ~1.32 ± 0.04, 0.62 ± 0.02, 0.42 ± 0.02, 0.12 ± 0.01, and 0.04 ± 0.01 MPa, corresponding to n:1 = 10:1, 15:1, 20:1, 30:1, and 40:1, respectively. When n:1 = 10:1 and 15:1, the obtained $PDMS_{(n:1)}$ microspheres after the above whole process still display smooth surfaces and have no visible differences from the original as-synthesized and OP-exposed microspheres (Figure 5a,b and Figure S1a,b). With a further increase of n:1 to 20:1, shallow dents can be identified on relatively larger $PDMS_{(20:1)}$ microspheres (Figure 5c). When n:1 = 40:1, the wrinkling behavior on the microsphere surfaces is similar to that on the $PDMS_{(30:1)}$ microspheres, although there is severe adhesion between the deformed $PDMS_{(40:1)}$ microspheres (Figure 5d). This surface morphological evolution with $E_{PDMS(n:1)}$ originates from the intimate dependence of σ_c^R and swelling degree on the microsphere modulus $E_{PDMS(n:1)}$.

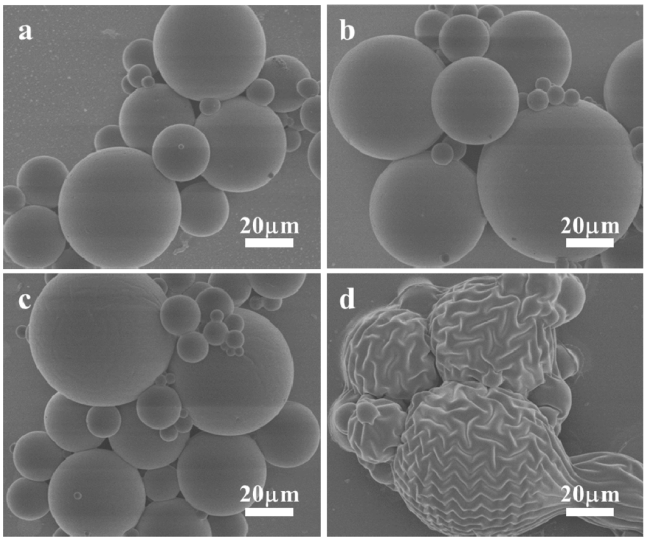

Figure 5. SEM images of $PDMS_{(n:1)}$ microspheres with different n:1 ratios for t_{OP} = 10 min followed by MMA swelling. n:1 = 10:1 (a), 15:1 (b), 20:1 (c), and 40:1 (d).

As shown in Figure 3d, r_D increases with a decrease of the cross-linking density and the stiffness of the PDMS microspheres (i.e., an increase of n:1). Note that the r_D values from n:1 = 40:1 approximately overlap with those from n:1 = 30:1 (Figure 3a,d), demonstrating that the swelling extent has reached a saturated state relative to the applied solvent. As mentioned above, the larger the swelling extent of the OP-treated PDMS microspheres, the larger the induced compressive stress in the shell/core spherical system correspondingly. Specifically, a decrease of the modulus by increasing n:1 not only enhances the induced compressive stress σ^R, but also decreases the required σ_c^R, facilitating the formation of surface wrinkles on the relatively soft microspheres (Figures 2, 4, and 5d). After drying of the microspheres in the atmosphere, the r_D values from n:1 = 10:1, 15:1, and 20:1 nearly collapse into the line of r_D = 0 (Figure 3d). With respect to the $PDMS_{(30:1)}$ and $PDMS_{(40:1)}$ microspheres, negative r_D values are obtained after air drying (Figure 3a,d), indicating a partial loss of the uncured molecules in these relatively soft PDMS microspheres during the swelling step. Additionally, the same power-law behavior between λ^R and R comes out on both $PDMS_{(30:1)}$ and $PDMS_{(40:1)}$ microspheres (Figure 2g and Figure S3b). Likewise, the microsphere modulus $E_{PDMS(n:1)}$ is implicitly reflected in the C_i (i = 1, 2, 3, 4) from eqs 4−7, having no influence on the slope values. Consequently, in the double logarithmic coordinate system, the λ^R−R plots for different $E_{PDMS(n:1)}$ values should be parallel to each other, as shown in Figure 2g. Certainly, the surface wrinkles on stiffer $PDMS_{(30:1)}$ microspheres have a smaller λ^R under the same conditions (Figure 2g and Figure S3b). Evidently, the microsphere modulus plays a crucial role in the spherical wrinkling behavior, which offers a good opportunity to actively modulate the spherical wrinkle morphologies.

In the above investigation, we have controlled the internal microstructures of the shell/core spherical system (e.g., R, $E_{PDMS(n:1)}$, h_R) to manipulate σ_c^R, σ^R, and the corresponding σ^R/σ_c^R. Consequently, promoting/restraining spherical wrinkling as well as tuning the wrinkle morphologies has been realized. Indeed, σ^R can be independently modulated in a quite simple way by external solvents of different swelling capacities. Here several typical solvents, including cyclohexane, toluene, acetone, and ethanol, have been explored (Figure 6). It is found that the radius range of PDMS microspheres that is allowed for spherical wrinkling is relatively wide in the case of cyclohexane and toluene (Figure 6a,b). When acetone and ethanol are used, surface wrinkling only happens on relatively large microspheres by contrast (Figure 6c,d). Specifically, when the cross-linked PDMS microspheres are immersed into the organic solvents, the solvent molecules can penetrate into the PDMS microsphere networks and swell the PDMS microspheres. According

DOI: 10.1021/acs.jpcb.5b07208
J. Phys. Chem. B 2015, 119, 13450−13461

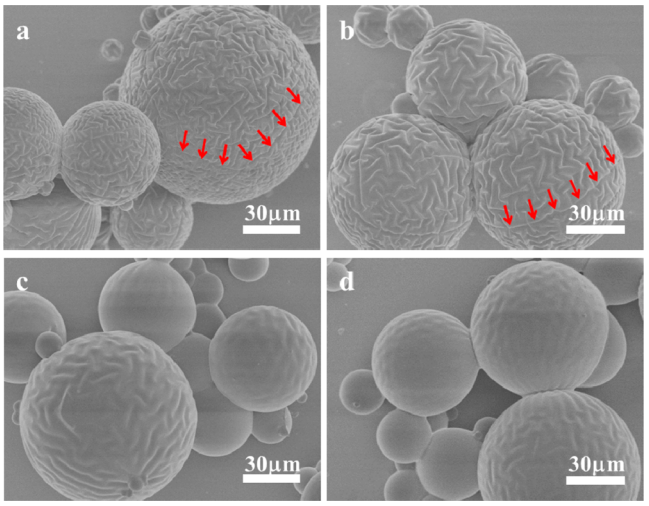

Figure 6. SEM images of $PDMS_{(30:1)}$ microspheres for t_{OP} = 10 min when different organic swelling solvents were employed: (a) cyclohexane, (b) toluene, (c) acetone, and (d) ethanol.

to Flory–Huggins theory, the mixed free energy (ΔG_M) of organic solvents and PDMS can be estimated as

$$\Delta G_M = kT\left(\frac{\phi_i}{N_i}\ln\phi_i + \frac{\phi_{PDMS}}{N_{PDMS}}\ln\phi_{PDMS} + \chi\phi_i\phi_{PDMS}\right) \quad (9)$$

where ϕ_i, ϕ_{PDMS}, N_i, N_{PDMS}, and χ represent the volume fractions of the organic solvent and PDMS, the numbers of lattice sites occupied by the organic solvent and PDMS, and the Flory–Huggins interaction parameter, respectively. T and k represent temperature and the Boltzmann constant, respectively.[42] Only when $\Delta G_M < 0$ can the organic solvent spontaneously swell the PDMS, and the degree of swelling can be determined by χ between the organic solvent and PDMS. Additionally, the real interaction parameter χ_{i-PDMS}, based on the solubility parameters of the organic solvent and PDMS, can be estimated as

$$\chi_{i-PDMS} = \frac{v_0(\delta_i - \delta_{PDMS})^2}{R_g T} \quad (10)$$

where v_0, δ_i, δ_{PDMS}, and R_g represent the lattice site volume, the solubility parameters of the organic solvents and PDMS, and the gas constant, respectively.[42] The solubility parameters of the involved organic solvent and PDMS are listed in Figure 3f. It is known that $\chi_{ethanol-PDMS} > \chi_{acetone-PDMS} > \chi_{toluene-PDMS} > \chi_{MMA-PDMS} > \chi_{cyclohexane-PDMS}$. It is noteworthy that χ reflects the variation of the interaction energy when the polymer and solvent or polymer and polymer are mixed. The smaller the value of χ, the stronger the interaction between the polymer and solvent, implying that this solvent is a good solvent for the polymer. Here χ decreases gradually for ethanol, acetone, toluene, MMA, and cyclohexane, respectively, and the interactions with the PDMS microspheres follow the opposite sequence. In other words, the swelling degree of the PDMS microspheres increases correspondingly from ethanol to cyclohexane, which shows good consistency with the measured results in Figure 3a,e, except a slight deviation from those for MMA and toluene. This deviation could be attributed to the nonpolarity of toluene and greater affinity for PDMS. Thus, the values of χ between solvents and OP-treated PDMS microspheres decrease with a decrease of $E_{PDMS(n:1)}$ and t_{OP}, further leading to an increase of the swelling degree of the OP-treated PDMS microspheres (Figure 3c,d). It is known that the macroscopic swelling degree of the PDMS microspheres can be clarified in terms of the microscopic molecule interaction parameter χ. At the same time, the swelling degree of the PDMS microspheres determines the ultimate excess stress exerted on the PDMS core/shell microspheres, which plays a crucial role in the wrinkle morphologies. Therefore, an intimate connection between the molecular parameter χ and the wrinkle patterns observed has been established. Specifically, the smaller the χ, the stronger the molecule interaction, the larger the swelling degree and the excess stress exerted on the PDMS microspheres, and finally the easier it is for the ridge-based wrinkle morphologies (herringbone or labyrinth patterns) to emerge on the PDMS microsphere surfaces (Figures 2–6). A further careful examination shows that labyrinthine patterns predominantly occur on the PDMS microspheres when cyclohexane and toluene are used (Figure 6a,b), while under the same conditions, the herringbone wrinkles are preferable from MMA swelling (Figures 2c, 4a–c, and 5d). These unexpected results are presumably related to the larger r_D values of cyclohexane and toluene (e.g., $r_{D(cyclohexane)}$ = 80–100%) compared to MMA (Figure 3a,e), which engenders some cracks (indicated by red arrows in Figure 6a,b) and further influences the stress-relief-based wrinkle morphologies. Furthermore, the λ^R–t_{OP} relationship corresponding to different solvents has also been plotted, which shows that the solvent nature has no apparent influence on the wrinkling wavelength λ^R (Figure S3a).

It is well-known that the outstanding characteristics of the spherical wrinkling compared to planar wrinkling are the curvature and overstress-sensitive wrinkle morphologies. Figure 7 exhibits a phase diagram of the wrinkle morphologies on PDMS microspheres under different experimental conditions. In this diagram, the horizontal coordinate is the normalized radius of curvature R/h_R and the vertical coordinate is the excess swelling degree (Figure 7). Here we use the excess swelling degree to roughly stand for the excess stress, which is defined as the difference between the swelling degree r_D under

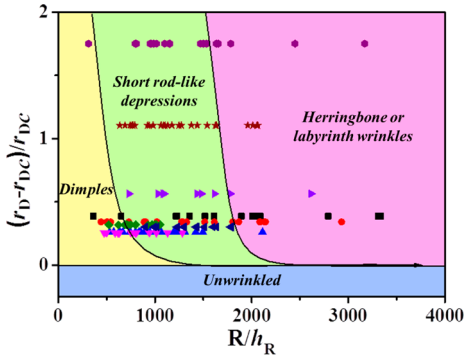

Figure 7. Phase diagram of wrinkle morphologies on PDMS microspheres under different experimental conditions: (1) $PDMS_{(30:1)}$ microspheres were exposed for t_{OP} = 5 min (squares), 10 min (circles), 15 min (tilted squares), 20 min (left-pointing triangles), 25 min (upright triangles), and 30 min (inverted triangles), followed by MMA swelling; (2) $PDMS_{(40:1)}$ microspheres were exposed for t_{OP} = 10 min, followed by MMA swelling (right-pointing triangles); (3) $PDMS_{(30:1)}$ microspheres were exposed for t_{OP} = 10 min, followed by toluene (stars) or cyclohexane (hexagons) swelling.

DOI: 10.1021/acs.jpcb.5b07208
J. Phys. Chem. B 2015, 119, 13450–13461

certain experimental conditions (Figure 3a,c–e) and the critical swelling degree r_{DC} divided by the critical swelling degree r_{DC} (i.e., $(r_D - r_{DC})/r_{DC}$). The critical swelling degree r_{DC} required for surface wrinkling on the PDMS microsphere surfaces is approximately assumed to be equal to the induced swelling degree of the PDMS microspheres with shallow depressions rather than the common wrinkles, such as $PDMS_{(20:1)}$ microspheres subjected to OP and MMA swelling. The normalized radius of curvature of the PDMS microspheres, R/h_R, needs the SiO_x layer thickness for different t_{OP} values, which can be calculated by the corresponding planar PDMS film wrinkling equation with the known λ, E_f, E_s, ν_f and ν_s. This phase diagram of wrinkle morphologies is analogous to that recently reported in the literature.[31] Namely, ordered dimples preferentially appear on the spherical surfaces in the case of a smaller radius of curvature and a smaller excess swelling degree, whereas typical herringbone or labyrinth morphologies are mainly self-assembled in the case of a larger radius of curvature or a larger excess swelling degree.

In the end, it is worthwhile to emphasize that the current spherical wrinkles induced via the combination of OP exposure and solvent swelling have some unique properties, e.g., memory effect, good reversibility, and stability, which are very important for the related applications. For example, when the OP-exposed PDMS microspheres are subjected to swelling sequentially in two different organic solvents, i.e., MMA and cyclohexane, the triggered wrinkling morphologies are mainly dependent on the first employed swelling agent (Figure S4), which is simply referred to as the memory effect here. Currently, the underlying physics for this memory effect in the wrinkle feature is not clear to us; however, it could be taken as an effective indicator of the applied organic solvent. Similar to those of the experimental system designed by Breid et al. in the PDMS caps exposed to UV/ozone and then ethanol vapor swelling,[26] the surface wrinkles fabricated by our combined method are also reversible, as evidenced via in situ optical observation (Figure S5). Namely, when MMA is dropped on the as-wrinkled $PDMS_{(30:1)}$ microspheres, the microspheres will immediately inflate, and subsequently the surface wrinkles disappear. Upon MMA evaporation, the approximately same wrinkle patterns are restored on the microspheres. In UVO-treated PDMS caps, the ethanol vapor preferentially swells the oxidized surface layer more than the underlying PDMS core, and then the swollen oxidized layer experiences an equi-biaxial compression due to the confinement of the PDMS inner core. Once the compressive stress reaches a critical value, wrinkles are formed spontaneously on the PDMS caps. After evaporation of ethanol, compressive stress is relieved, leading to the recovery of the smooth surfaces. Surface wrinkles could appear again when the ethanol vapor is recovered. As for the OP-treated PDMS microspheres here, the employed organic solvents (e.g., MMA, toluene, cyclohexane) are good swelling agents for PDMS. Therefore, there are some differences between these two approaches. For example, the positions in which the employed solvents work are different: one is the oxidized surface layer, and the other is the PDMS inner core. In addition, solvent evaporation makes the UVO-treated PDMS caps smooth, while surface wrinkles on the OP-treated PDMS microspheres exist without organic solvents. Additionally, the induced wrinkle morphologies via combination of OP exposure and solvent treatment are stable in the air, satisfying the application demand in the long run.

CONCLUSIONS

In summary, spontaneous formation of surface wrinkling patterns on a curved substrate provides a simple, quick, and cost-effective method to fabricate and manipulate microstructures, which could complement conventional fabrication techniques, especially in fabricating real 3D nonplanar structures. In this paper, we present a general and versatile approach to generate surface wrinkles on spherical surfaces via the combination of OP exposure and solvent swelling. Specifically, the normalized substrate radius of curvature R/h_R and the overstress σ^R/σ_c^R collectively dictate the surface wrinkle morphologies with typically dimples, short rodlike depressions, and labyrinthine and herringbone patterns. Here, R/h_R and σ^R/σ_c^R could be well tailored by the radius size R, Young's modulus of the PDMS microspheres $E_{PDMS(n:1)}$, the shell thickness h_R (i.e., the OP exposure duration t_{OP}), and the organic solvent nature. It is found that the wrinkling wavelength λ^R and the microsphere radius R show the power-law behavior for different t_{OP} and $E_{PDMS(n:1)}$ values. The corresponding phase diagram of the wrinkle morphologies on the spherical surfaces vs the normalized radius of curvature R/h_R and the excess swelling degree $[(r_D - r_{DC})/r_{DC}]$ has been demonstrated. Apparently, this introduced spherical wrinkling method enables patterning arbitrarily curved surfaces inaccessible to other techniques. It is believed that the ability to tune these highly ordered wrinkling patterns makes these wrinkles excellent candidates for tunable multifunctional surface properties such as friction, adhesion,[43] wetting or dewetting, and cell growth. On the other hand, the rich results reported here could benefit the understanding of the stress-driven morphogenesis of some natural soft materials and tissues in terms of mechanical views, which are also promising for applications in biological scaffolds, intelligent materials,[44] and therapeutics, such as the inhibition of tumor development and invasion.[22,25]

ASSOCIATED CONTENT

Supporting Information

The Supporting Information is available free of charge on the ACS Publications website at DOI: 10.1021/acs.jpcb.5b07208.

SEM images of as-synthesized $PDMS_{(n:1)}$ microspheres with n:1 = 10:1, 15:1, 20:1, and 40:1 (Figure S1), optical images of OP-exposed $PDMS_{(30:1)}$ microspheres in the swelling and dried states (Figure S2), λ^R–t_{OP} relationship corresponding to different $E_{PDMS(n:1)}$ values and organic solvents and lg λ^R–lg R relationship corresponding to different $E_{PDMS(n:1)}$ and t_{OP} values (Figure S3), influence of sequential processing in MMA and cyclohexane on the resulting wrinkles (Figure S4), and investigation of the stability and reversibility of the as-formed wrinkles (Figure S5) (PDF)

In situ optical observation of OP-exposed $PDMS_{(30:1)}$ microspheres after a droplet of MMA is dropped (Movie S1) (AVI)

AUTHOR INFORMATION

Corresponding Author

*E-mail: chlu@tju.edu.cn

Author Contributions

†Q.L., X.H., and J.H. contributed equally to this work.

Notes

The authors declare no competing financial interest.

DOI: 10.1021/acs.jpcb.5b07208
J. Phys. Chem. B 2015, 119, 13450–13461

■ ACKNOWLEDGMENTS

Financial support from the National Natural Science Foundation of China (Grants 21074090 and 21374076) and Tianjin Research Program of Application Foundation and Advanced Technology (Grant 13JCYBJC17100) is gratefully acknowledged. We also acknowledge Prof. Cao Yanping (Tsinghua University, Beijing, People's Republic of China) for the characterization of the moduli of planar PDMS films with different *n*:1 ratios before and after solvent extraction.

■ REFERENCES

(1) Chan, E. P.; Crosby, A. J. Fabricating Microlens Arrays by Surface Wrinkling. *Adv. Mater.* **2006**, *18*, 3238−3242.
(2) Chandra, D.; Yang, S.; Lin, P.-C. Strain Responsive Concave and Convex Microlens Arrays. *Appl. Phys. Lett.* **2007**, *91*, 251912.
(3) Howarter, J. A.; Stafford, C. M. Instabilities as a Measurement Tool for Soft Materials. *Soft Matter* **2010**, *6*, 5661−5666.
(4) Chung, J. Y.; Nolte, A. J.; Stafford, C. M. Surface Wrinkling: A Versatile Platform for Measuring Thin-Film Properties. *Adv. Mater.* **2011**, *23*, 349−368.
(5) Khang, D.-Y.; Jiang, H.; Huang, Y.; Rogers, J. A. A Stretchable Form of Single-Crystal Silicon for High-Performance Electronics on Rubber Substrates. *Science* **2006**, *311*, 208−212.
(6) Khang, D.-Y.; Rogers, J. A.; Lee, H. H. Mechanical Buckling: Mechanics, Metrology, and Stretchable Electronics. *Adv. Funct. Mater.* **2009**, *19*, 1526−1536.
(7) Lu, C.; Möhwald, H.; Fery, A. A Lithography-Free Method for Directed Colloidal Crystal Assembly Based on Wrinkling. *Soft Matter* **2007**, *3*, 1530−1536.
(8) Yin, J.; Lu, C. Hierarchical Surface Wrinkles Directed by Wrinkled Templates. *Soft Matter* **2012**, *8*, 6528−6534.
(9) Genzer, J.; Groenewold, J. Soft Matter with Hard Skin: From Skin Wrinkles to Templating and Material Characterization. *Soft Matter* **2006**, *2*, 310−323.
(10) Bowden, N.; Brittain, S.; Evans, A. G.; Hutchinson, J. W.; Whitesides, G. M. Spontaneous Formation of Ordered Structures in Thin Films of Metals Supported on an Elastomeric Polymer. *Nature* **1998**, *393*, 146−149.
(11) Bowden, N.; Huck, W. T. S.; Paul, K. E.; Whitesides, G. M. The Controlled Formation of Ordered, Sinusoidal Structures by Plasma Oxidation of an Elastomeric Polymer. *Appl. Phys. Lett.* **1999**, *75*, 2557−2559.
(12) Huck, W. T. S.; Bowden, N.; Onck, P.; Pardoen, T.; Hutchinson, J. W.; Whitesides, G. M. Ordering of Spontaneously Formed Buckles on Planar Surfaces. *Langmuir* **2000**, *16*, 3497−3501.
(13) Yang, Y.; Han, X.; Ding, W.; Jiang, S.; Cao, Y.; Lu, C. Controlled Free Edge Effects in Surface Wrinkling via Combination of External Straining and Selective O_2 Plasma Exposure. *Langmuir* **2013**, *29*, 7170−7177.
(14) Ding, W.; Yang, Y.; Zhao, Y.; Jiang, S.; Cao, Y.; Lu, C. Well-Defined Orthogonal Surface Wrinkles Directed by the Wrinkled Boundary. *Soft Matter* **2013**, *9*, 3720−3726.
(15) Yoo, P. J. Invited Paper: Fabrication of Complexly Patterned Wavy Structures Using Self-Organized Anisotropic Wrinkling. *Electron. Mater. Lett.* **2011**, *7*, 17−23.
(16) Guo, C. F.; Nayyar, V.; Zhang, Z.; Chen, Y.; Miao, J.; Huang, R.; Liu, Q. Path-Guided Wrinkling of Nanoscale Metal Films. *Adv. Mater.* **2012**, *24*, 3010−3014.
(17) Moon, M.-W.; Lee, S. H.; Sun, J.-Y.; Oh, K. H.; Vaziri, A.; Hutchinson, J. W. Controlled Formation of Nanoscale Wrinkling Patterns on Polymers Using Focused Ion Beam. *Scr. Mater.* **2007**, *57*, 747−750.
(18) Moon, M. W.; Lee, S. H.; Sun, J. Y.; Oh, K. H.; Vaziri, A.; Hutchinson, J. W. Wrinkled Hard Skins on Polymers Created by Focused Ion Beam. *Proc. Natl. Acad. Sci. U. S. A.* **2007**, *104*, 1130−1133.
(19) Yin, J.; Chen, X.; Sheinman, I. Anisotropic Buckling Patterns in Spheroidal Film/Substrate Systems and Their Implications in Some Natural and Biological Systems. *J. Mech. Phys. Solids* **2009**, *57*, 1470−1484.
(20) Cao, G.; Chen, X.; Li, C.; Ji, A.; Cao, Z. Self-Assembled Triangular and Labyrinth Buckling Patterns of Thin Films on Spherical Substrates. *Phys. Rev. Lett.* **2008**, *100*, 036102.
(21) Yin, J.; Bar-Kochba, E.; Chen, X. Mechanical Self-Assembly Fabrication of Gears. *Soft Matter* **2009**, *5*, 3469−3474.
(22) Chen, X.; Yin, J. Buckling Patterns of Thin Films on Curved Compliant Substrates with Applications to Morphogenesis and Three-Dimensional Micro-Fabrication. *Soft Matter* **2010**, *6*, 5667−5680.
(23) Li, B.; Jia, F.; Cao, Y.-P.; Feng, X.-Q.; Gao, H. Surface Wrinkling Patterns on a Core-Shell Soft Sphere. *Phys. Rev. Lett.* **2011**, *106*, 234301.
(24) Trindade, A. C.; Canejo, J. P.; Pinto, L. F. V.; Patrício, P.; Brogueira, P.; Teixeira, P. I. C.; Godinho, M. H. Wrinkling Labyrinth Patterns on Elastomeric Janus Particles. *Macromolecules* **2011**, *44*, 2220−2228.
(25) Li, B.; Cao, Y.-P.; Feng, X.-Q.; Gao, H. Mechanics of Morphological Instabilities and Surface Wrinkling in Soft Materials: A Review. *Soft Matter* **2012**, *8*, 5728−5745.
(26) Breid, D.; Crosby, A. J. Curvature-Controlled Wrinkle Morphologies. *Soft Matter* **2013**, *9*, 3624−3630.
(27) Jeong, Y.; Chen, Y.-C.; Turksoy, M. K.; Rana, S.; Tonga, G. Y.; Creran, B.; Sanyal, A.; Crosby, A. J.; Rotello, V. M. Tunable Elastic Modulus of Nanoparticle Monolayer Films by Host-Guest Chemistry. *Adv. Mater.* **2014**, *26*, 5056−5061.
(28) Terwagne, D.; Brojan, M.; Reis, P. M. Smart Morphable Surfaces for Aerodynamic Drag Control. *Adv. Mater.* **2014**, *26*, 6608−6611.
(29) Yin, J.; Han, X.; Cao, Y.; Lu, C. Surface Wrinkling on Polydimethylsiloxane Microspheres via Wet Surface Chemical Oxidation. *Sci. Rep.* **2014**, *4*, 5710.
(30) Bae, H. J.; Bae, S.; Park, C.; Han, S.; Kim, J.; Kim, L. N.; Kim, K.; Song, S.-H.; Park, W.; Kwon, S. Biomimetic Microfingerprints for Anti-Counterfeiting Strategies. *Adv. Mater.* **2015**, *27*, 2083−2089.
(31) Stoop, N.; Lagrange, R.; Terwagne, D.; Reis, P. M.; Dunkel, J. Curvature-Induced Symmetry Breaking Determines Elastic Surface Patterns. *Nat. Mater.* **2015**, *14*, 337−342.
(32) Cai, S.; Breid, D.; Crosby, A. J.; Suo, Z.; Hutchinson, J. W. Periodic Patterns and Energy States of Buckled Films on Compliant Substrates. *J. Mech. Phys. Solids* **2011**, *59*, 1094−1114.
(33) Trindade, A. C.; Canejo, J. P.; Patrício, P.; Brogueira, P.; Teixeira, P. I.; Godinho, M. H. Hierarchical Wrinkling on Elastomeric Janus Spheres. *J. Mater. Chem.* **2012**, *22*, 22044−22049.
(34) Zhao, T.; Qiu, D. One-Pot Synthesis of Highly Folded Microparticles by Suspension Polymerization. *Langmuir* **2011**, *27*, 12771−12774.
(35) Yang, M.; Guo, Y.; Wu, Q.; Luan, Y.; Wang, G. Synthesis and Properties of Amphiphilic Nonspherical SPS/PS Composite Particles by Multi-Step Seeded Swelling Polymerization. *Polymer* **2014**, *55*, 1948−1954.
(36) Liu, S.; Deng, R.; Li, W.; Zhu, J. Polymer Microparticles with Controllable Surface Textures Generated through Interfacial Instabilities of Emulsion Droplets. *Adv. Funct. Mater.* **2012**, *22*, 1692−1697.
(37) Bayley, F. A.; Liao, J. L.; Stavrinou, P. N.; Chiche, A.; Cabral, J. T. Wavefront Kinetics of Plasma Oxidation of Polydimethylsiloxane: Limits for Sub-μm Wrinkling. *Soft Matter* **2014**, *10*, 1155−1166.
(38) Nania, M.; Matar, O. K.; Cabral, J. T. Frontal Vitrification of PDMS using Air Plasma and Consequences for Surface Wrinkling. *Soft Matter* **2015**, *11*, 3067−3075.
(39) Han, X.; Zhao, Y.; Cao, Y.; Lu, C. Controlling and Prevention of Surface Wrinkling via Size-Dependent Critical Wrinkling Strain. *Soft Matter* **2015**, *11*, 4444−4452.
(40) Glatz, B. A.; Tebbe, M.; Kaoui, B.; Aichele, R.; Kuttner, C.; Schedl, A. E.; Schmidt, H.-W.; Zimmermann, W.; Fery, A. Hierarchical Line-Defect Patterns in Wrinkled Surfaces. *Soft Matter* **2015**, *11*, 3332−3339.

DOI: 10.1021/acs.jpcb.5b07208
J. Phys. Chem. B 2015, 119, 13450−13461

(41) Jiang, K.; Thomas, P. C.; Forry, S. P.; DeVoe, D. L.; Raghavan, S. R. Microfluidic Synthesis of Monodisperse PDMS Microbeads as Discrete Oxygen Sensors. *Soft Matter* **2012**, *8*, 923−926.
(42) Zhang, X.; He, Y.; Wang, Y. The Continuous Exudation of Micro-Meniscus Capsules by Polymer Perspiration. *Adv. Mater. Interfaces* **2015**, *2*, 1400474.
(43) Kundu, S.; Davis, C. S.; Long, T.; Sharma, R.; Crosby, A. J. Adhesion of Nonplanar Wrinkled Surfaces. *J. Polym. Sci., Part B: Polym. Phys.* **2011**, *49*, 179−185.
(44) Xie, J.; Han, X.; Zong, C.; Ji, H.; Lu, C. Large-Area Patterning of Polyaniline Film Based on *in Situ* Self-Wrinkling and Its Reversible Doping/Dedoping Tunability. *Macromolecules* **2015**, *48*, 663−671.

DOI: 10.1021/acs.jpcb.5b07208
J. Phys. Chem. B 2015, 119, 13450−13461